

WHU-PA3D: Qaidam Basin Planetary Analogous-3D Dataset

Ang Jin^{1,2,3}, Chi Chen^{1,2,3*}, Yuhang Xu^{1,2,3}, Yangzi Cong⁴, Weitong Wu⁵, Liuchun Li⁶, Yifan Li^{1,2,3}, Bisheng Yang^{1,2,3}

¹ State Key Laboratory of Information Engineering in Surveying, Mapping and Remote Sensing, Wuhan University, Wuhan 430079, China- (angjin, chichen, yuhangxu, yifan.l, bshyang)@whu.edu.cn

² Engineering Research Center for Spatio-temporal Data Smart Acquisition and Application, Ministry of Education of China, Wuhan University, Wuhan 430079, China

³ Institute of Geo-spatial intelligence, Wuhan University, Wuhan 430079, China

⁴ School of Space Science and Technology, Shandong University, Weihai, 264209, China-(yzcong)@sdu.edu.cn

⁵ School of Earth Sciences and Engineering, Hohai University, Nanjing, 211100, China-(weitongwu)@hhu.edu.cn

⁶ Institute of Artificial Intelligence, School of Computer Science, Wuhan University, Wuhan 430079, China- (LiuC.Lee)@whu.edu.cn

Keywords: Planetary exploration, Unstructured environments, LiDAR, SLAM, Image classification.

Abstract

Accurate localization and detailed environmental perception are critical for planetary exploration, particularly in unstructured and complex terrains. To support such efforts, we present the WHU-PA3D dataset, a planetary analog dataset collected in the Mars-like Qaidam Basin. This dataset includes eight handheld LiDAR point cloud sequences and seven UAV image sequences, documenting diverse terrains such as yardangs, water-eroded landscapes, and canyons. It integrates multimodal data, including RGB imagery, LiDAR, and IMU measurements, offering a realistic testing platform for SLAM and image classification algorithms. Benchmarking experiments reveal the strengths and limitations of existing algorithms in handling complex and unstructured environments. The WHU-PA3D dataset provides a useful reference for planetary surface localization, geological analysis, and mission planning.

1. Introduction

1.1 General Instructions

With the rapid advancement of space science and technology, the demand for exploration of planetary surfaces has become increasingly urgent. Planetary surface localization and mapping, as a critical task, provides accurate navigation maps for planetary rovers and other equipment. This is of great significance for planning safe and efficient exploration routes, identifying resources, and establishing human habitats and infrastructure for activities (Wynne et al., 2022). Traditional planetary rovers typically rely on stereo cameras and other equipment, but the advantage of LiDAR lies in its reliable performance in low-light conditions, ensuring effective surface mapping even in environments with insufficient lighting. It can capture subtle surface changes and topographic features, providing robust data support for scientific research on planetary geology and landforms.

Currently, LiDAR point cloud-based SLAM technology has achieved successful applications in various fields such as autonomous driving (Bresson et al., 2017; Bürki et al., 2019; Cong et al., 2023), automated construction (Mascaro et al., 2021), and agriculture (Oliveira et al., 2021; Shu et al., 2021), enabling accurate localization and map construction in unknown environments. However, SLAM performance still requires further evaluation when dealing with unstructured and highly complex environments (Giubilato et al., 2022a; Le Gentil et al., 2020). Particularly on planetary surfaces such as the Moon and Mars, their unique and complex terrain features—such as craters, mountains, and fissures on the Moon, and deserts and canyons on Mars—lack structured features like buildings or roads, making localization and map construction significantly more challenging.

In the field of general LiDAR SLAM, datasets like KITTI (Geiger et al., 2013) have become standard benchmarks for evaluating algorithm performance. However, they are primarily limited to urban environments and man-made structures, and fall short when addressing SLAM challenges such as feature degradation and scene complexity in natural environments. To address these issues, researchers have developed LiDAR SLAM datasets specifically for natural environments, such as forests, rugged terrain, underground mines, lakes, and farms (Leung et al., 2017). To better meet the demands of planetary surface LiDAR SLAM, purpose-designed datasets have now emerged. These datasets simulate the extreme environments of planetary surfaces and provide challenging topographical features. Tong CH et al. (Tong et al., 2013) provided two real planetary simulation rover test scenarios, with data collected by different rover platforms using a stop-scan-go method to gather 3D laser scan data, where $360^\circ \times 180^\circ$ full-range scans are performed when the rover is stationary. Table 1 summarizes some existing SLAM datasets for unstructured scenes.

However, despite these datasets providing more realistic environments for planetary exploration missions, there are still some unresolved challenges. To better meet the demands of planetary surface LiDAR SLAM, we present a dataset collected in the Qaidam Basin of Qinghai, China. The Qaidam Basin is renowned for its unusual natural geography and unique geological formations and is widely regarded as one of the most "Mars-like" places on Earth. We recorded eight point cloud sequences using a handheld sensor unit, with durations ranging from 5 to 18 minutes and covering distances up to approximately 2 kilometers. The unit included two RGB wide-angle cameras, LiDAR, and IMU. Additionally, seven UAV image sequences were collected using a DJI drone, covering the point cloud collection scenarios mentioned above. The eight point cloud sequences collected by the handheld device and the seven image sequences collected by the UAV were classified

* Corresponding author

based on different terrains, including yardang landforms and water erosion landforms. To further validate the application value of the dataset, we designed specific experiments to test the capabilities of 3D reconstruction, SLAM, and image classification algorithms. First, we processed UAV images to generate high-precision 3D models. These models can simulate

the realistic terrain of planetary surfaces, assisting researchers in conducting navigation and localization experiments under various conditions. Secondly, we conducted benchmarking experiments on the dataset, including LiDAR-SLAM and aerial image classification. Through the above research, we aim to provide robust data support for planetary exploration missions.

Table 1: SLAM Datasets in Unstructured Environments

Datasets	Sensors	Quantity	Length	Platform
(Leung et al., 2017)	Stereo Camera, 3D LiDAR, 2D Radar	43	~2km	Rover
(Furgale et al., 2012)	Stereo Camera, Sun Sensor, Inclinometer	23	~10km	Rover
(Meyer et al., 2021)	Stereo Camera, RGB Camera, Omnidirectional Camera	36	~9.2km	Handheld
(Vayugundla et al., 2018)	Stereo Camera	2	~2km	Rover
(Giubilato et al., 2022b)	Stereo Camera, 3D LiDAR	7	~4.3km ~90min	Handheld
(Hewitt et al., 2018)	Stereo Camera, 3D LiDAR, ToF Camera, UAV Visible Light	3	~1.8km ~87min	Rover, UAV
Ours	RGB Camera, 3D LiDAR, UAV Visible Light and Infrared	15	~4.5km ~95min	Handheld, UAV

2. Datasets

In the Qaidam Basin of western China, we collected eight point cloud sequences and seven UAV image sequences, documenting the unique features of various natural geological and landform characteristics in the region. The Qaidam Basin is renowned for its distinctive natural geography and geological structure, and is widely regarded as one of the most "Mars-like" places on Earth. Figure 1 shows the hardware devices used in our data collection.



Figure 1: Handheld Scanner and UAV Used for Data Collection

2.1 Data collection devices

The handheld sensor system integrates a VLP16 LiDAR and an MTI-300 IMU. The VLP16 LiDAR features a 360-degree horizontal field of view and a 30-degree vertical field of view (-15° to +15°), operating at 10 Hz. The MTI-300 IMU provides high-quality inertial measurements with a roll/pitch accuracy of

0.2° RMS, heading accuracy of 1° RMS. Additionally, two visible-light cameras in the system capture RGB images at resolutions of 1920×1080 pixels, with a 220-degree horizontal field of view.

The UAV system captures high-resolution terrain imagery using visible-light and infrared cameras. The visible-light camera features an 85° field of view, a 35 mm equivalent focal length of 24 mm, and an aperture of f/2.8. Images are captured at a resolution of 4056×3040 pixels, with automated flight planning ensuring an overlap rate of 80% laterally and 70% longitudinally. The infrared camera provides thermal imaging with a resolution of 640×480 pixels and captures temperature ranges of -10°C to +140°C in high-gain mode or -10°C to +400°C in low-gain mode. The GNSS module supports GPS+GLONASS dual-satellite positioning, achieving positional accuracy of ±0.5 m vertically and ±1.5 m horizontally during flight.

2.2 Data introduction

The data collection area is remote from human activity, offering us an view of extreme and undisturbed natural environments, including landforms commonly found on Mars, such as yardang and water erosion features. In terms of yardang landforms, we collected three point cloud sequences and two UAV image sequences. These point cloud sequences capture the complex and towering yardang formations and significant topographical variations, making them suitable for testing the pose estimation capability of SLAM algorithms in complex terrains.

In terms of water erosion landforms, we collected four point cloud sequences and five UAV image sequences. These point cloud sequences encompass the complex structures of gully and river valley landforms, resembling water erosion landforms on Mars. By analyzing erosion features, river channels, and valley networks in these point cloud data, researchers can gain deeper

insights into the origins and movement processes of Martian water bodies (Xiao, 2021).

Additionally, we collected one point cloud sequence in a canyon. Compared to other terrains, canyons are a typical structural landform with significant faulting, folding, and geological features.

To provide a comprehensive overview of the data collection, Table 2 summarizes the handheld LiDAR data collection sequences in the Qaidam Basin, while Table 3 details the corresponding UAV data collection sequences. Additionally, all

UAV data were processed using DJI Terra software to generate 3D models, including both mesh and point cloud models. Notably, the Yardang01 handheld sequence corresponds directly to the Yardang01 UAV sequence, capturing the same region through complementary perspectives. Similarly, the handheld sequences Yardang02-03 align with the UAV sequence Yardang02. The handheld sequences Gully01-03 correspond to the UAV sequences Gully01-03, and the handheld sequence River Valley 01 is consistent with the UAV sequences River Valley01-02.

Table 2: Overview of Handheld LiDAR Data Collection Sequences in the Qaidam Basin

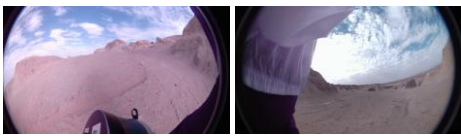
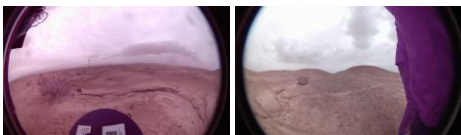
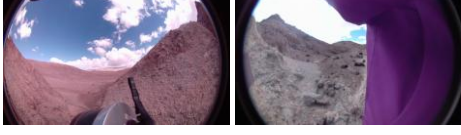
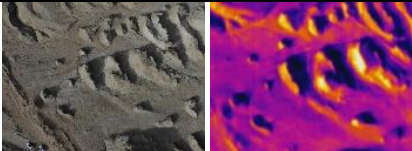
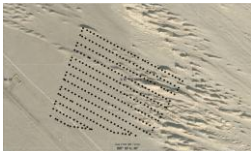
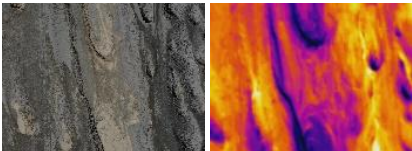
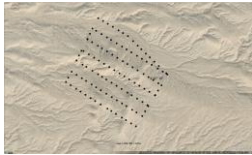
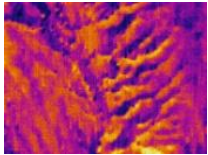
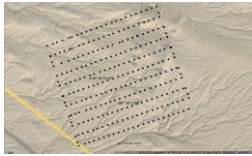
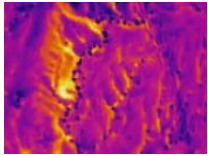
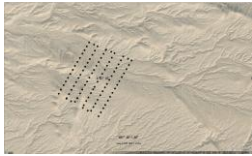
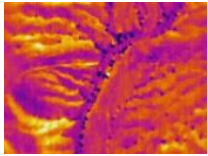
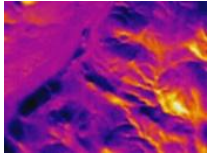
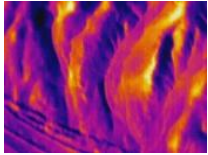
RosBag Filename	Duration	Handheld Device Image Samples	Description
Yardang01	315 sec		Yardang landscape, data collected along the base of formations (Approx. 0.23 km).
Yardang02	908 sec		Yardang landscape, data collected along the base of formations (Total approx. 1.02 km).
Yardang03	521 sec		
Gully01	1118 sec		Water erosion landforms (Gullies) in Qaidam Basin. (Total approx. 1.82 km)
Gully02	1077 sec		
Gully03	434 sec		
River Valley01	356 sec		Water erosion landforms (River Valley) in Qaidam Basin. (approx. 0.19 km)
Canyon01	1013s	N/A	Collected in a canyon; no trajectory and camera malfunction, only point clouds recorded.

Table 3: Overview of UAV Data Collection Sequences in the Qaidam Basin

Name	Quantity	Area (km ²)	D-GPS Trajectory	Data Samples
Yardang01	63	0.0614		
Yardang02	339	0.3255		

Gully 01	116	0.1330			
Gully 02	217	0.2970			
Gully 03	95	0.1193			
River Valley 01	271	0.2150			
River Valley 02	143	0.2063			

3. Benchmark

To evaluate the performance of existing SLAM and image processing algorithms in planetary-like environments, we conducted comprehensive benchmarking on the WHU-PA3D dataset, including performance assessment of LiDAR-SLAM algorithms and experimental analysis of image classification tasks.

3.1 SLAM

To evaluate the performance of existing SLAM algorithms in planetary-like environments, we conducted experiments on some mainstream LiDAR odometry algorithms (Lv et al., 2021; Xu et al., n.d.; Zhang and Singh, 2014) using the WHU-PA3D dataset. Because most of our data were collected in natural, unstructured terrains, where artificial features are largely absent, standard SLAM algorithms encountered substantial difficulties. In our experiments, we observed that many solutions either struggled to initialize or maintain tracking in regions with sparse or repetitive geometry, yielding partial or inconsistent results.

Among these approaches, LOAM (Zhang and Singh, 2014) successfully processed a short portion of the "Canyon01" sequence, yet it exhibited trajectory instability and produced incomplete maps in areas with abrupt morphological changes. Figure 2 illustrates LOAM's localization trajectory and generated point cloud map in the canyon sequence. While the system performed adequately in segments featuring more prominent terrain structures, its accuracy degraded rapidly over extended stretches lacking sufficient vertical constraints.

A range of underlying factors contribute to these challenges. Specifically, planetary-analog terrains typically feature fewer

distinct geometric cues, making it difficult for feature-based matching algorithms to remain reliable over extended trajectories. Environmental conditions such as dust, variable lighting, and highly uneven topography further compromise sensor measurements and reduce SLAM robustness. Looking ahead, two major directions for improvement can be pursued: (1) hardware advancements, for example integrating LiDAR sensors with increased channel counts or larger vertical fields of view to capture more comprehensive surface information, and (2) algorithmic refinements, which may involve leveraging multi-modal data fusion (e.g., LiDAR, camera, and IMU) and designing more robust feature-extraction and matching strategies tailored to unstructured geological settings.

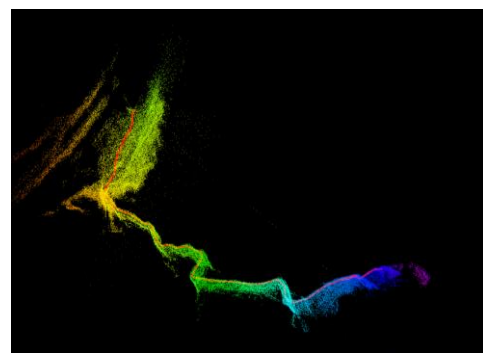


Figure 2: Localization Trajectory and Map in the Canyon Sequence (LOAM)

3.2 Image Classification

The dataset contains a total of 1,244 high-resolution images, with 622 images used for the training set and 622 images used for the test set. Due to the spatial overlap of the UAV-collected data, random splitting may result in training and test sets being too similar, which could hinder the effective evaluation of the

model's generalization ability. Therefore, we divided the data based on the range and time of capture to ensure that the training and test sets do not overlap spatially.

To comprehensively evaluate the classification performance of models on planetary-like terrains, we selected mainstream deep learning image classification models, including the ResNet (He et al., 2016) (ResNet-34, ResNet-50, ResNet-101), VGG (Simonyan and Zisserman, 2015), EfficientNet (Tan and Le, 2019), Vision Transformer (Dosovitskiy et al., 2021), and models integrating convolutional and Transformer architectures, such as SwinV2 (Liu et al., 2022) (SwinV2-small, SwinV2-tiny), MaxViT (Tu et al., 2022) and VOLO (Yuan et al., 2021). The selection of these models was primarily based on their lightweight design and efficiency, making them suitable for resource-constrained and real-time processing scenarios in planetary exploration missions. Moreover, these models encompass both classic convolutional neural network (CNN) architectures and modern Transformer architectures, enabling a comprehensive evaluation of their performance in image classification for planetary-like terrains.

During the experiments, all models were trained under the same settings. We used cross-entropy as the loss function, with SGD as the optimizer and a learning rate of 0.1. The training batch size was set to 16, and a total of 75 epochs were conducted. All models were implemented and trained using the PyTorch framework, with acceleration provided by an NVIDIA RTX 3060 GPU. To comprehensively evaluate the classification performance of the model, we used the F1-score as the primary evaluation metric, which combines both precision and recall.

Experimental results (Table 4) indicate that existing image classification algorithms face challenges in planetary-like environments, particularly in distinguishing between categories with similar terrain features. Future research could consider the following aspects: First, increasing dataset diversity by collecting more images under varying lighting conditions, seasons, and angles to enhance model generalization. Second, integrating multimodal data such as multispectral and infrared imagery to enrich feature representations and improve the model's ability to discern subtle differences. Additionally, designing specialized network architectures for terrain features or incorporating attention mechanisms to enhance feature learning in critical areas are also promising directions for exploration.

Table 4: Image Classification F1-score of the Dataset

Method	Params	Yardang	Gully	River Valley
resnet34	21.8	95.59	95.93	92.44
resnet50	25.56	85.97	91.40	62.50
resnet101	44.55	90.81	90.03	68.79
vgg19	143.68	83.33	93.47	74.41
Maxvits(tiny)	30.92	92.59	99.27	89.12
swinv2(small)	49.7	96.05	97.83	88.96
swinv2(tiny)	28.33	93.26	96.27	73.79
Efficientnet(b0)	5.29	85.07	97.31	80.94
Vit(tiny)	5.72	86.86	91.10	60.98
volo(d1)	26.63	94.20	98.53	80.71

4. Conclusion

We present a dataset recorded in a planetary simulation environment, which includes camera, LiDAR, and Inertial Measurement Unit (IMU) data, covering several typical natural geological and landform features, such as yardang landforms, water erosion landforms, and canyons. We also evaluated the performance of various LiDAR-based SLAM algorithms and the classification performance of aerial images on the sequences. This dataset provides a realistic testing platform for positioning and navigation technologies in planetary exploration missions, and also offers valuable data resources for geological and landform analysis as well as planetary environment simulation.

Acknowledgements

This research was funded by the National Natural Science Foundation of China (No.U22A20568), the National Key RESEARCH and Development Program (No.2022YFB3904101), the Fundamental Research Funds for the Central Universities. This research was supported by LIESMARS Special Research Funding. (Corresponding author: Chi Chen).

The part numerical calculations in this paper have been done on the supercomputing system in the Supercomputing Center of Wuhan University.

References

- Bresson, G., Alsayed, Z., Yu, L., Glaser, S., 2017. Simultaneous Localization and Mapping: A Survey of Current Trends in Autonomous Driving. *IEEE Transactions on Intelligent Vehicles* 2, 194–220. <https://doi.org/10.1109/TIV.2017.2749181>
- Bürki, M., Schaupp, L., Dymczyk, M., Dubé, R., Cadena, C., Siegart, R., Nieto, J., 2019. VIZARD: Reliable Visual Localization for Autonomous Vehicles in Urban Outdoor Environments, in: 2019 IEEE Intelligent Vehicles Symposium (IV). Presented at the 2019 IEEE Intelligent Vehicles Symposium (IV), pp. 1124–1130. <https://doi.org/10.1109/IVS.2019.8814017>
- Cong, Y., Chen, C., Yang, B., Liang, F., Ma, R., Zhang, F., 2023. CAOM: Change-aware online 3D mapping with heterogeneous multi-beam and push-broom LiDAR point clouds. *ISPRS Journal of Photogrammetry and Remote Sensing* 195, 204–219. <https://doi.org/10.1016/j.isprsjprs.2022.11.017>
- Dosovitskiy, A., Beyer, L., Kolesnikov, A., Weissenborn, D., Zhai, X., Unterthiner, T., Dehghani, M., Minderer, M., Heigold, G., Gelly, S., Uszkoreit, J., Houlsby, N., 2021. An Image is Worth 16x16 Words: Transformers for Image Recognition at Scale. <https://doi.org/10.48550/arXiv.2010.11929>
- Furgale, P., Carle, P., Enright, J., Barfoot, T.D., 2012. The Devon Island rover navigation dataset. *The International Journal of Robotics Research* 31, 707–713. <https://doi.org/10.1177/0278364911433135>
- Geiger, A., Lenz, P., Stiller, C., Urtasun, R., 2013. The KITTI Vision Benchmark Suite. *The KITTI Vision Benchmark Suite* 1–13.
- Giubilato, R., Gentil, C.L., Vayugundla, M., Schuster, M.J., Vidal-Calleja, T., Triebel, R., 2022a. GPGM-SLAM: a Robust

- SLAM System for Unstructured Planetary Environments with Gaussian Process Gradient Maps. *FR* 2, 1721–1753. <https://doi.org/10.55417/fr.2022053>
- Giubilato, R., Stürzl, W., Wedler, A., Triebel, R., 2022b. Challenges of SLAM in Extremely Unstructured Environments: The DLR Planetary Stereo, Solid-State LiDAR, Inertial Dataset. *IEEE Robotics and Automation Letters* 7, 8721–8728. <https://doi.org/10.1109/LRA.2022.3188118>
- He, K., Zhang, X., Ren, S., Sun, J., 2016. Deep residual learning for image recognition, in: *Proceedings of the IEEE Conference on Computer Vision and Pattern Recognition*. pp. 770–778.
- Hewitt, R.A., Boukas, E., Azkarate, M., Pagnamenta, M., Marshall, J.A., Gasteratos, A., Visentin, G., 2018. The Katwijk beach planetary rover dataset. *The International Journal of Robotics Research* 37, 3–12. <https://doi.org/10.1177/0278364917737153>
- Le Gentil, C., Vayugundla, M., Giubilato, R., Stürzl, W., Vidal-Calleja, T., Triebel, R., 2020. Gaussian Process Gradient Maps for Loop-Closure Detection in Unstructured Planetary Environments, in: *2020 IEEE/RSJ International Conference on Intelligent Robots and Systems (IROS)*. Presented at the 2020 IEEE/RSJ International Conference on Intelligent Robots and Systems (IROS), pp. 1895–1902. <https://doi.org/10.1109/IROS45743.2020.9341667>
- Leung, K., Lühr, D., Houshiar, H., Inostroza, F., Borrmann, D., Adams, M., Nüchter, A., Ruiz Del Solar, J., 2017. Chilean underground mine dataset. *The International Journal of Robotics Research* 36, 16–23. <https://doi.org/10.1177/0278364916679497>
- Liu, Z., Hu, H., Lin, Y., Yao, Z., Xie, Z., Wei, Y., Ning, J., Cao, Y., Zhang, Z., Dong, L., Wei, F., Guo, B., 2022. Swin Transformer V2: Scaling Up Capacity and Resolution. <https://doi.org/10.48550/arXiv.2111.09883>
- Lv, J., Hu, K., Xu, J., Liu, Y., Ma, X., Zuo, X., 2021. CLINS: Continuous-Time Trajectory Estimation for LiDAR-Inertial System, in: *2021 IEEE/RSJ International Conference on Intelligent Robots and Systems (IROS)*. Presented at the 2021 IEEE/RSJ International Conference on Intelligent Robots and Systems (IROS), pp. 6657–6663. <https://doi.org/10.1109/IROS51168.2021.9636676>
- Mascaro, R., Wermelinger, M., Hutter, M., Chli, M., 2021. Towards automating construction tasks: Large-scale object mapping, segmentation, and manipulation. *Journal of Field Robotics* 38, 684–699. <https://doi.org/10.1002/rob.22007>
- Meyer, L., Smíšek, M., Fontan Villacampa, A., Oliva Maza, L., Medina, D., Schuster, M.J., Steidle, F., Vayugundla, M., Müller, M.G., Rebele, B., Wedler, A., Triebel, R., 2021. The MADMAX data set for visual-inertial rover navigation on Mars. *Journal of Field Robotics* 38, 833–853. <https://doi.org/10.1002/rob.22016>
- Oliveira, L.F.P., Moreira, A.P., Silva, M.F., 2021. Advances in Agriculture Robotics: A State-of-the-Art Review and Challenges Ahead. *Robotics* 10, 52. <https://doi.org/10.3390/robotics10020052>
- Shu, F., Lesur, P., Xie, Y., Pagani, A., Stricker, D., 2021. SLAM in the Field: An Evaluation of Monocular Mapping and Localization on Challenging Dynamic Agricultural Environment. Presented at the *Proceedings of the IEEE/CVF Winter Conference on Applications of Computer Vision*, pp. 1761–1771.
- Simonyan, K., Zisserman, A., 2015. Very Deep Convolutional Networks for Large-Scale Image Recognition. <https://doi.org/10.48550/arXiv.1409.1556>
- Tan, M., Le, Q., 2019. EfficientNet: Rethinking Model Scaling for Convolutional Neural Networks, in: *Proceedings of the 36th International Conference on Machine Learning*. Presented at the International Conference on Machine Learning, PMLR, pp. 6105–6114.
- Tong, C.H., Gingras, D., Larose, K., Barfoot, T.D., Dupuis, É., 2013. The Canadian planetary emulation terrain 3D mapping dataset. *The International Journal of Robotics Research* 32, 389–395. <https://doi.org/10.1177/0278364913478897>
- Tu, Z., Talebi, H., Zhang, H., Yang, F., Milanfar, P., Bovik, A., Li, Y., 2022. MaxViT: Multi-Axis Vision Transformer. <https://doi.org/10.48550/arXiv.2204.01697>
- Vayugundla, M., Steidle, F., Smisek, M., Schuster, M.J., Bussmann, K., Wedler, A., 2018. Datasets of Long Range Navigation Experiments in a Moon Analogue Environment on Mount Etna, in: *ISR 2018; 50th International Symposium on Robotics*. Presented at the ISR 2018; 50th International Symposium on Robotics, pp. 1–7.
- Wynne, J.J., Titus, T.N., Agha-Mohammadi, A., Azua-Bustos, A., Boston, P.J., de León, P., Demirel-Floyd, C., De Waele, J., Jones, H., Malaska, M.J., Miller, A.Z., Sapers, H.M., Sauro, F., Sonderegger, D.L., Uckert, K., Wong, U.Y., Alexander Jr., E.C., Chiao, L., Cushing, G.E., DeDecker, J., Fairén, A.G., Frumkin, A., Harris, G.L., Kearney, M.L., Kerber, L., Léveillé, R.J., Manyapu, K., Massironi, M., Mylroie, J.E., Onac, B.P., Parazynski, S.E., Phillips-Lander, C.M., Prettyman, T.H., Schulze-Makuch, D., Wagner, R.V., Whittaker, W.L., Williams, K.E., 2022. Fundamental Science and Engineering Questions in Planetary Cave Exploration. *Journal of Geophysical Research: Planets* 127, e2022JE007194. <https://doi.org/10.1029/2022JE007194>
- Xiao, L., 2021. *Mars On Earth: A Study Of The Qaidam Basin*. World Scientific.
- Xu, W., Cai, Y., He, D., Lin, J., Zhang, F., n.d. FAST-LIO2: Fast Direct LiDAR-inertial Odometry 1– 19.
- Yuan, L., Hou, Q., Jiang, Z., Feng, J., Yan, S., 2021. VOLO: Vision Outlooker for Visual Recognition. <https://doi.org/10.48550/arXiv.2106.13112>
- Zhang, J., Singh, S., 2014. LOAM: Lidar Odometry and Mapping in Real-time., in: *Robotics: Science and Systems*. pp. 1–9.